A step forward towards demystifying sleep physiology: Dominant screening of sleep and wake behavior in mice

著者（英）	Kim StaciJakyong
year	2019
その他のタイトル	フォワード・ジェネティクスで同定した新規睡眠制御遺伝子解明
学位授与大学	筑波大学 (University of Tsukuba)
学位授与年度	2019
報告番号	12102甲第9253号
URL	http://doi.org/10.15068/00158040

筑 波 大 学

University of Tsukuba

博 士（人間生物学）学 位 論 文

Ph.D. dissertation in Human Biology

A step *forward* towards demystifying sleepy physiology:

Dominant screening of sleep and wake behavior in mice

（フォワード・ジェネティクスで同定した新規睡眠制御遺伝子解明）

2019

筑波大学グローバル教育院

School of Integrative Global Majors in University of Tsukuba

Ph.D. Program in Human Biology

STACI JAKYONG KIM

"... for he grants sleep to those he loves"

Psalms 127:2

ACKNOWLEDGMENTS

First, I would like to thank my advisor, Professor Masashi Yanagisawa, for unwavering support. He has always been considerate of every outcome and obstacles and steered me in the right direction. Also, to the members of my dissertation committee: Professor Akira Shibuya, Dr. Joseph Takahashi, and Dr. Kaspar Vogt. I feel extremely blessed to work with such wonderful teachers.

This dissertation is a product of a great teamwork. I want to thank all present and past members of the Yanagisawa/Funato lab. Many deserving thanks to the ENU group members, especially Dr. Hiromasa Funato and Dr. Chika Miyoshi. Dr. Funato has guided me every step of the way since I joined the project, never failed to inspire me as an aspiring researcher. Dr. Chika Miyoshi, with her nurturing character, pulled me through the demanding days of mouse colony management and screening. I must express appreciation for Ms. Miyo Kakizaki and Ms. Noriko Hotta for the exceptional craftsmanship of mouse work they taught me. I am also thankful for Ms. Aya Ikkyu and Ms. Satomi Kanno for their assistance in the strenuous molecular experiments. This laborious screening study could not have been possible without the hard work of one and each member of the team.

I want to take this opportunity to acknowledge Dr. Shigeharu Wakana and Dr. Takahiro Ezaki for their support and the expertise they brought into this project.

I give special thanks to my parents, my husband, my pastors and church family for their love and encouragement. I could not have achieved anything without their spiritual support and prayers. I am blessed with such a faithful and trusting family, always cheering me to pursue my dream.

ABSTRACT

The sleep-wake cycle is an intricate process controlled by a complex cascade of effectors. The homeostatic propensity to sleep increases as "sleep need" accumulates during the wakeful state, driving animals to commence in sleep behavior. However, the molecular and cellular mechanism that facilitates such a switch is largely unknown. In an attempt to identify the regulatory cascade of sleep and wake behavior, we established a large-scale screening system based on EEG and EMG using mice to employ forward genetics approach.

Our high-throughput screening system follows the dominant screening scheme of randomly mutagenized mice, which possesses major advantages when compared to the more conventional recessive screening scheme. This paper discusses the theoretical basis for the study and presents the details of the methodology and workflow.

In addition to *Sleepy* and *Dreamless* mutants reported by Funato *et al*., our study continues to reveal more candidate genes, including *Cacna1a* showing a mild decrease in total wake time resulting from a heterozygous mutation. Based on the parameters tested, our screening system is modifiable for application in any behavioral analysis other than sleep/wakefulness.

TABLE OF CONTENTS

LIST OF ABBREVIATIONS

As	A-single spermatogonia
B10J	C57BL/10J
B6J	C57BL/6J
B6N	C57BL/6N
CRISPR	Clustered regularly interspaced short palindromic repeats
CV	Coefficient of variance
EEG	Electroencephalogram
EMG	Electromyogram
ENU	N-ethyl-N-nitrosourea
LOD	Logarithm of odds
NREM	Non-rapid-eye-movement
QTL	Quantitative trait loci
REM	Rapid-eye-movement
SD	Standard deviation
SNP	Single nucleotide polymorphism

LIST OF FIGURES AND TABLES

Figures Page

Tables

LIST OF PRIOR PUBLICATIONS

Funato, H., Miyoshi, C., Fujiyama, T., Kanda, T., Sato, M., Wan, Z., Ma, J., Nakane, S., Tomita, J., Ikkyu, A., Kakizaki, M., Hotta-Hirashima, N., Kanno, S., Komiya, H., Asano, F., Honda, T., Kim, S.J., Harano, K., Muramoto, H., Yonezawa, T., Mizuno, S., Miyazaki, S., Connor, L., Kumar, V., Miura, I., Suzuki, T., Watanabe, A., Abe, M., Sugiyama, F., Takahashi, S., Sakimura, K., Hayashi, Y., Liu, Q., Kume, K., Wakana, Shigeharu., Takahashi, J.S., Yanagisawa, M. Forward-genetics analysis of sleep in randomly mutagenized mice. *Nature* 539, 378–383, 2016.

Hossain, M.S., Asano, F., Fujiyama, T., Miyoshi, C., Sato, M., Ikkyu, A., Kanno, S., Hotta, N., Kakizaki, M., Honda, T., Kim, S.J., Komiya, H., Miura, I., Suzuki, T., Kobayashi, K., Kaneda, H., Kumar, V., Takahashi, J.S., Wakana, Shigeharu., Funato, H., Yanagisawa, M. Identification of mutations through dominant screening for obesity using C57BL/6 substrains. *Scientific Reports*. 6, 32453, 2016.

Kang, J.M., Park, S., Kim, S.J., Kim, H., Lee, B., Kim, J., Park, J., Kim, S.T., Yang, H.K., Kim, W.H., Kim, S.J. KIAA1324 Suppresses Gastric Cancer Progression by Inhibiting the Oncoprotein GRP78. *Cancer Research* 75(15), 3087–3097, 2015.

Park, S., Kang, J.M., Kim, S.J., Kim, H., Hong, S., Lee, Y.J., and Kim, S.J. Smad7 enhances ATM activity by facilitating the interaction between ATM and Mre11-Rad50-Nbs1 complex in DNA double-strand break repair. *Cell. Mol. Life Sci*. 72(3), 583–596. 2015.

Kim, T.A., Kang, J.M., Hyun, J.S., Lee, B., Kim, S.J., Yang, E.S., Hong, S., Lee, H.J., Fujii, M., Niederhuber, J.E., Kim, S.J. The Smad7-Skp2 complex orchestrates Myc stability, impacting on the cytostatic effect of TGF-β. *J. Cell Sci*. 127, 411–421. 2014.

Kang, J.M., Park, S., Kim, S.J., Hong, H.Y., Jeong, J., Kim, H.S., Kim, S.J. CBL enhances breast tumor formation by inhibiting tumor suppressive activity of TGF-β signaling. *Oncogene*. 31, 5123-5131, 2012.

SECTION I: INTRODUCTION

Sleep is a ubiquitous behavior; no species in the animal kingdom with central nervous system has been demonstrated to sustain life without sleep or a sleep-like quiescent state. Mammalian sleep exhibits a cyclic transition between rapid eye movement sleep (REMS) and non-REM sleep (NREMS), defined by the characteristic brain activity and muscle tone, as measured by electroencephalogram (EEG) and electromyogram (EMG), respectively. Although recent advances in the optogenetic and chemogenetic manipulation of neurons have led to the accumulation of information about executive neural circuitries regulating sleep and wake states (Weber and Dan, 2016), the molecular and cellular mechanisms that drive the switch between wakefulness, NREMS and REMS remain a mystery.

In an attempt to unravel the regulatory mechanism of sleep and wake behavior, we established a large-scale sleep screening system based on EEG and EMG using mice to employ forward genetics approach. This research strategy follows an unbiased phenotypic screening to find the causal genetic relationship with the inherited trait. The first utilization of forward genetics in behavioral biology dates to 1970s when *Drosophila melanogaster* was screened for aberrant phenotypes after treatment with mutagens, leading to groundbreaking discoveries including identification of the *period* gene (Citri et al., 1987; Konopka and Benzer, 1971; Reddy et al., 1984). Later, the *Clock*

gene was discovered in mice using a similar approach for the first time (King et al., 1997), contributing hugely to the current understanding of the circadian clock system (Ripperger et al., 2011; Takahashi, 2016). Ever since the discovery that flies exhibit behavior states that qualify as sleep/wakefulness (Hendricks et al., 2000; Shaw, 2000), an intensive effort has been made to decipher sleep through the fly genetics (Tomita et al., 2017). Currently in flies, however, sleep can only be assessed through monitoring the locomotive activities. It is unclear whether sleep in flies is truly analogous to mammalian sleep, in which the gold standard in defining and assessing sleep is through EEG/EMG analysis.

The advantages in using mice over fruit flies in sleep research include the capability in reliably staging three vigilance states, wakefulness, NREMS and REMS through EEG/EMG-based somnography analysis. Furthermore, the homology of the genome and brain structure between mouse and human predicts a conserved mechanism regulating sleep/wakefulness. We expect that findings in mice can be applied to human sleep physiology and pathology. For example, since its discovery in 1998, *Orexin* has been well established as an essential regulator of wakefulness. Orexin-deficient mice show multidimensional phenotypic aberration that is similar to a human sleep disorder, narcolepsy (Chemelli et al., 1999; Volpe and Ratan, 2007). This led to the understanding of the pathophysiology of the disorder and to the development of a novel class of drug for insomnia (Coleman et al., 2017). Thus, the use of mouse models has facilitated extension into understanding

human disease and drug discoveries, further emphasizing the utility of the murine model in translational studies.

Nonetheless, there are obstacles when undertaking a large-scale forward genetic study using adult mice in comparison to simpler organisms, such as *D. melanogaster* or *Caenorhabditis elegans*. Mice have generation time of at least three months, which is considerably longer than the flies (10-12 days), and must be kept under a tightly controlled environment. This requires a high maintenance cost for husbandry and labor-intensive. Also, the high-throughput sleep analysis needs well-trained research staff for implantation surgery and EEG/EMG-based sleep staging. Despite these difficulties, advances in bioinformatics and genome editing over the last 10 years have improved the speed and feasibility of the forward genetics research in mice. Since the completion of the whole mouse genome sequencing (Chinwalla et al., 2002), a tremendous pool of information on the genetic background of inbred mouse strains is available including a genome-wide list of genetic markers between B6J and B6N (Kumar et al., 2013). Traditionally, counter strains genetically very distant from the mutagenized strain were preferred because polymorphic markers were more readily available. However, use of such distant counter strains became unnecessary allowing us to use mutagenized and counter strains with genetic proximity and near-identical phenotype (Funato et al., 2016; Hossain et al., 2016). Most of the phenotype-inducing mutations are a single nucleotide substitution that lie within the coding regions. Thus, whole-exome sequencing combined with coarse

linkage analyses can immediately provide a list of candidate gene mutations. Importantly, the technical advances in nuclease-mediated targeted mutagenesis, such as CRISPR/Cas9 system, facilitates efficient examination of causality of an identified mutation.

This paper describes the methods and workflow for the large-scale, high-throughput screening of randomly mutagenized mice for sleep and wake behavior. We also provide a theoretical discussion on the relationship among the logarithm of odds (LOD) score, statistical significance and the extent of the sleep phenotype. In addition, a new pedigree, *Drowsy*, which carries a mutation in the *Cacna1a* gene is described. Our screening scheme and statistical simulation of the phenotype is modifiable for any type of behavior and physiological screening other than sleep/wakefulness.

SECTION II: RESULTS AND DISCUSSION

2.1 Animal selection

It is strategically and practically desirable to select an appropriate age of animals to minimize housing and maintenance cost. Screening younger mice may reduce the cost of husbandry, but it poses risk that young mice may exhibit immature sleep and wake behavior (Nelson et al., 2013). Considering the vulnerability to implantation surgery and maturity of the skull, we performed the implantation surgery at 9-10 weeks of age and EEG/EMG recording after 7-10 days of recovery. Only male mice were screened for the strategic advantage as the number of sperms from a single male mouse is greater than that of eggs from one female mouse, and sperm can be cryopreserved relatively easily. Also, male mice are preferred in behavioral studies due to the chance of estrous cycle serving as a potential confounding factor in female mice, and therefore only a few studies have examined sleep/wakefulness in female mice (Komiya et al., 2018).

2.2 Choice of inbred strain

The proper choice of inbred strains for mutagenized fathers and counter-strain mothers is one of the most crucial factors for a successful screening. Each inbred strain shows a characteristic sleep/wake behavior (Franken et al., 1998, 2001; Tafti et al., 1999), which is attributed to the presence of many quantitative trait loci (QTL). A wide variance may mask the effect of ENU-

induced mutations if two strains are not chosen carefully. We selected B6J as mutagenized strain and B6N as counter strain because they are very close to each other (separated only ~70 years ago) (Figure 1), yet the whole-genome sequences and a list of single nucleotide polymorphism (SNP) markers were available (Chinwalla et al., 2002; Kumar et al., 2013). However, we noticed inconsistent SNPs in each substrain derived from different breeders. Multiple substrains were sequenced to generate an evenly distributed list of 96 SNPs (Figure 2, Table 1) (Mekada et al., 2015).

To evaluate the similarity in the sleep/wakefulness between B6J and B6N, we examined two strains against B10J. Consistent with the genetic proximity, B6J and B6N showed similar time spent in wakefulness, NREMS and REMS, whereas B10J exhibited a shorter daily wake time accounted by change in total sleep time (Figure 3A-C). Second parameter examined were the episode duration of each vigilance state. Although B6J and B6N showed similar episode duration over 24-h in wakefulness and NREMS, the REMS episode durations in B6N mice was longer during the light phase and shorter during the dark phase (Figure 3D-F). EEG power spectrum analysis showed a similar trend in B6J, B6N, and B10J during NREMS and REMS (Figure 3G-H). There was no significant difference in the delta power (1-4 Hz) density during NREMS or the theta power (6-9 Hz) density during REMS (Figure 3I-J). We also examined the response to sleep deprivation in each substrain. During the 18-h recovery sleep following the 6-h sleep deprivation from ZT0-6, the total time spent in wake during dark phase was slightly but

significantly longer in B6N with decrease in both NREMS and REMS (Figure 4A-C). The increase in the NREMS and REMS time during dark phase was similar in B6J and B6N, but significantly lower in B10J (Figure 4D). The NREMS EEG delta power during the first 6 h after sleep deprivation was slightly but significantly smaller in B6N (Figure 4E). Although this suggest that B6N may have maginally blunted homeostatic response to sleep deprivation, it would be difficult to map the causal loci because of the relatively poor reproducibility of these parameters (see below).

Since the difference in sleep/wakefulness between B6J and B6N strains is very small, the use of the two strains as mutagenized and counter strains is optimal for forward genetics of sleep and presumably suitable for other behavioral and metabolic traits (Kumar et al., 2013). Indeed, this combination enabled us to identify, for the first time, obesogenic mutations through dominant screening (Hossain et al., 2016).

2.3 ENU dosage and mutagenic effect

ENU has been the choice for random mutagenesis study in mice because of its high potency but relatively weak lethality (Hitotsumachi et al., 1985; Russell et al., 1979). After the administration of ENU, mice enter a temporary sterile condition because the mutagen targets the spermatogonia. The loss and regaining of fertility are good indication of the mutagenic effect and induction of random mutations. The recovery time is variable depending on the dosage and mouse strain. B6 mice regain fertility after 8-12 weeks but

now with sperms carrying the ENU-induced mutations. An appropriate dosage must be set to avoid a long-term influence of this potent mutagen that may deteriorate the health of the animal. Conversely, too low a dose would induce only a small number of mutations.

The initial ENU administration of 85mg/kg body weight twice at weekly interval resulted in 50-70 mutations per haploid exome in the F1 as examined by whole exome sequencing (data not shown). However, many of the G0 mutagenized mice remained fertile. The ENU dosage was optimized based on the updated standard protocol of weekly injections of 100 mg/kg body weight ENU (Hitotsumachi et al., 1985; Russell et al., 1979). At the age of 8 to 10 weeks, male B6J mice were treated with weekly intraperitoneal injection of ENU for three weeks based on the Mutagenetix protocol (http://mutagenetix.utsouthwestern.edu) (Wang et al., 2015). The mutagenized mice were subjected to routine sterility check by cohabitating with wild-type female mice.

2.4 Screening strategy

Many of the large-scale forward genetics studies in the literatures follow the recessive screening scheme (Goldowitz et al., 2004). This requires breeding of three generations in each founder pedigree before proceeding to the phenotypic screening. The G3 progeny in recessive screening has a chance of either 1/16 (intercross scheme, shaded enclosure) or 1/8 (backcross scheme, dotted enclosure) (Figure 5A) to carry the homozygous mutation.

Typically, 30-50 G3 mice are screened per pedigree to reach statistical power for linkage analysis (Beutler et al., 2007) requiring a massive amount of resources. On the other hand, dominant screening follows simpler workflow, fewer generations from the mutagenesis to phenotype screening and a smaller colony size requirement for assessing the same number of gene mutations, since each F1 founder represents haploid genome of the mutagenized G0 father (Siepka and Takahashi, 2005).

In our dominant screening, F1 offspring from a cross between the mutagenized G0 father (B6J) and wild-type counter strain mother (B6N) is screened for sleep/wake phenotype. The F1 phenodeviant is subsequently backcrossed with wild-type B6N female to obtain N2 progeny for assessing heritability of the sleep abnormality (Figure 5B). In most cases (43 out of 57 pedigrees), the N2 generation did not inherit the presumptive phenotype seen in F1 and showed normal sleep/wake behavior (Figure 5C, Phenotype A). This may be due to a deviation by chance in F1 mice or a summed weak effect diluted by mating with wild-type mouse. When the inherited phenotype is subtle, the histogram of sleep parameters would be similar to the normal behavior making it difficult to determine the heritability (Figure 5C, Phenodeviant B). For a heritable weak-to-moderate sleep abnormality, the histogram showed two partially overlapped peaks of the sleep parameter, which allowed determining a small number of N2 mice as either phenodeviant or normal, and many remaining N2 mice undetermined (Figure 5C, Phenodeviant C). When the pedigree had a strong sleep

phenotype, two non-overlapped peaks of the sleep parameter enabled us to determine each N2 mice as phenodeviant and normal (Figure 5C, Phenodeviant D). We proceed to quantitative trait loci (QTL) analysis when at least 20% of the male N2 littermates are determined as phenodeviants.

Given that sleep parameters follow normal distribution, the expected incidence of mice outside 3 standard deviations (SD) is 0.003. At the early stage of our screening, no more than five phenodeviants were identified for every 1,000 mice, indicating that many of these "phenodeviants" happened by chance. The chance of establishing heritable phenodeviant pedigree would increase with the higher number of mice screened. Thus far, we have screened 10,024 mice and identified 57 phenodeviants. Out of the 57 pedigrees, 14 are confirmed for the heritability of the sleep phenotype and mutations mapped to 10 loci, including 5 pedigrees carrying the same *Sik3*^{Slp} allele (Funato et al., 2016). So far at least 4 independent causative gene mutations have been validated.

Strategically, dominant screening presents advantages over recessive screening that include simpler workflow and substantially less requirement of resources for mouse propagation and maintenance. The inherent challenge in dominant screening is the low frequency of obtaining mice showing the heritable phenotypes compared with recessive screening. This may partly be due to the presence of the wild-type allele or the low penetrance of the gene mutation (Nolan et al., 1997). Gain-of-function

mutations may sometimes fail to reflect the endogenous function of the gene of interest, especially in disease manifestation by a neomorphic type of allele. On the other hand, screens for dominant mutants will, in many instances, reveal semi-dominance of the allele. Some of these mutations are antimorphic in nature, and can be critical in understanding the gene's function as in the case of the *Clock* ENU mutant; the function of the *Clock* gene would never have been considered based on the knockout phenotype alone (DeBruyne et al., 2006; King et al., 1997). In addition, homozygous mutations often lead to lethality or severe disease, preventing examination of sleep/wake phenotype, as in the case of the *Cacna1a* (*Drowsy*) mutation (see below) (Hayasaka et al., 2017; Uebi et al., 2012). Indeed, genetic mutations identified in the heritable sleep disorder, such as familial advance sleep phase (FASP), show autosomal-dominant inheritance (Shi et al., 2017). Several genome-wide association studies (GWAS) also show heterozygous carriers of the polymorphism having altered sleep architectures (Goel, 2017).

2.5 Number of F1 mice derived from a single ENU-treated mouse

We considered the maximum number of F1 mice derived from each G0 mouse based on the diversity of the mutations in a single G0 mouse sperm. Since the number of stem cell-like type A-single spermatogonia (A_S) is 35,000 per testis (Tagelenbosch and de Rooij, 1993) and a single injection of 100 mg/kg ENU kills more than 90% A_S spermatogonia (Oakberg and

Crosthwait, 1983), three serial treatment results in the survival of only 70 A_S spermatogonia. Since all sperm derived from a single spermatogonium have the same set of induced mutations, the number of surviving spermatogonia determines the number of different sets of mutations.

The expected number of distinct mutations in F1 mice derived from a single G0 mouse, $N_{\text{non-overlapped}}$, is theoretically given by

$$\boldsymbol{N_{\text{non-overlapped}} = N_{\text{sp}}\left[1 - \left(1 - \frac{1}{N_{\text{sp}}}\right)^{N_{\text{F1}}}\right]} \quad (1)$$

where N_{F1} and N_{sp} denote the number of F1 mice and the number of A_S in the G0 mouse remaining after ENU treatments, respectively. A formal derivation for this equation is as follows:

Let $P(M, N_{\text{F1}})$ be the probability of finding M non-overlapping mutations in N_{F1} individuals. $P(M, N_{\text{F1}})$ satisfies the following recursive formula,

$$P(M, N_{\text{F1}}) = P(M, N_{\text{F1}} - 1)\frac{M}{N_{\text{sp}}} + P(M-1, N_{\text{F1}} - 1)\left(1 - \frac{M-1}{N_{\text{sp}}}\right).$$

Thus, the expected number of M, $E[M; N_{\text{F1}}]$ (= $N_{\text{non-overlapped}}$), is written as

$$E[M; N_{\text{F1}}] = \sum_{M=1}^{N_{\text{F1}}} MP(M, N_{\text{F1}})$$

$$= \sum_{M=1}^{N_{\text{F1}}} M\left[P(M, N_{\text{F1}} - 1)\frac{M}{N_{\text{sp}}} + P(M-1, N_{\text{F1}} - 1)\left(1 - \frac{M-1}{N_{\text{sp}}}\right)\right]$$

$$= E[M; N_{\text{F1}} - 1]\left(1 - \frac{1}{N_{\text{sp}}}\right) + 1.$$

By solving this recursive formula with $E[M; 0] = 0$ and $E[M; 1] = 1$, we obtain Eq. (1).

We calculated the number of non-overlapping mutation sets with varying number of 10 to 200 F1 mice derived from an ENU-treated male (N_{F1}) with $N_{non\text{-}overlapped}$ for N_{SP} = 70 and 70,000 (Figure 6). When the number of F1 mice is small, the non-overlapping mutation sets increase proportionally to the number of F1 mice. As the number of F1 mice increases, the rate of increase is strongly suppressed by overlapping mutations. For this reason, we selected a moderate number of F1 mice (N = 60). Since the effect of ENU-treatment on G0 mice may not be constant, the number of overlapped mutations may show an upward trend. In our experience, the identical mutation in the *Sik3* genes was confirmed in five pedigrees derived from five founder mice among 60 offspring of a single G0 male (Funato et al., 2016). This was an exceptional case; no such duplication has been observed in other pedigrees. ENU might have particularly strong effects on this G0 mouse leaving very few spermatogonia survived, which severely limited the diversity of mutations in sperms.

2.6 Sleep/wakefulness screening parameters

Sleep/wake parameters that are suitable for sleep phenotyping must be highly reproducible in each mouse. Based on our experience, qualitative findings such as a loss of atonia during REMS or a disappearance of the theta wave during REMS tend to be stable in the same mouse. For quantitative

sleep parameters, such as the total time and episode duration, we tested reproducibility in the sleep/wakefulness of B6J mice by recording twice at more than four-week interval. The total time spent in wakefulness and NREMS of each mouse in the first recording significantly correlated with that in the second recording (Figure 7A-B), but not in the total REMS (Figure 7C). Episode duration of wakefulness and NREMS did not reproduce between the first and second recordings (Figure 7D-E). Interestingly, the REMS episode duration in the first recording significantly correlated with that in the second recording (Figure 7F). The total time spent in wakefulness and NREMS after 6-h of sleep deprivation by shaking the cages was not correlated between the first and second recordings (Figure 5G-H). The good reproducibility of the total wake time, total NREMS time and REMS episode duration was consistent with our experience that *Sik3*^{Sleepy} mutant and *Nacln*^{Dreamless} mutant pedigrees were isolated based on total wake/NREM sleep time and REM sleep episode duration, respectively (Funato et al., 2016).

Moreover, sleep parameters suitable for forward genetics research should exhibit minimal individual variability, indicated as the coefficient of variation (CV). For quantitative parameters, we selected mice with phenotypes that deviated from the average by approximately 3 SD with good reproducibility in the second recording. A parameter with a high CV is not suitable for behavioral screening because the distribution of mutants overlaps with normal mice. For example, the circadian period length was

very tightly regulated with CV = 0.0072, which is 50-fold lower than that of fear conditioning and the psychostimulant response (Takahashi et al., 2008), leading to successful application of forward genetics research. The CV of each parameters are summarized in Table 1. The smaller variation in total wake time (0.11), total NREMS time (0.13), and REMS episode duration (0.13) may further corroborate the successful establishment of *Sik3*^{Sleepy} mutant and *Nalcn*^{Dreamless} mutant pedigrees (Funato et al., 2016).

Table 1 CV of screening criteria

	Wake	NREMS	REMS
Total time	0.11	0.13	0.21
Episode duration	0.48	0.27	0.13
Delta power	--	0.23	--
Theta power	--	--	0.24

The EEG delta density during NREM sleep and the theta density during REM sleep also correlated well between the first and second recordings (Figure 5I-J). However, the variances were large, thus making the two sleep parameters unsuitable for forward genetic screening.

2.7 Proof of causality

Almost all phenotype-inducing gene mutations identified in ENU mutagenesis are amino-acid changing mutations identified in the coding regions (Beutler et al., 2007; Simon et al., 2015). Thus, whole-exome sequencing may be sufficient to detect responsible mutations in mutant pedigrees. Still, even though all candidate mutations in the heritable pedigrees so far mapped to coding

regions in our screening, we must consider the possibility that there may be causal mutations outside coding regions.

In some cases, whole-exome sequencing may reveal more than one candidate mutations within the mapped region. Although it is usually easy to select one gene from the candidate genes linked to the phenotype, proving that the other genes do not affect the phenotype could be a challenge. For example, we identified mutations in the *Sim1* gene (Chr10: 50908536) and *Sec63* gene (Chr10: 42816394) in an obesity pedigree (Hossain et al., 2016). Since SIM1 is known to cause obesity and mutant SIM1 protein did not function as a transcription factor, the *Sim1* mutation alone could explain the obesity. However, we could not positively deny the possibility that mutant SEC63 protein, which is involved in protein translocation at the ER membrane, may also affect body weight. In such cases, one way to establish causality would be to generate animals that are recombinants across this region; only one mutation will consistently segregate with the phenotype.

2.8 Probability of reaching significance

A QTL represents the genomic regions (loci) associated with a phenotype variation (quantitative trait). It is carried out by a statistical test to link the genetic mapping to a trait to produce the LOD score (van Ooijen, 1999). High LOD score indicates a high probability of a responsible gene mutation located in a particular chromosomal region (Wiltshire et al., 2002). To examine the relationship among the strength of sleep phenotype, number of

N2 mice examined and LOD score, a Monte Carlo simulation of the LOD score was performed for various population sizes of N2 mice (N_{N2} = 60, 80, and 120). The LOD score was computed based on surrogate data produced from the empirical data (23 control (+/+) mice and 37 mutant (m/+) mice) in the following manner.

(i) For each group, sample $N_{N2}/2$ individuals from the empirical data were selected uniformly at random allowing duplication. Note that here 50% of the population in the surrogate data is set to be mutants.

(ii) The mean wake time of each control mouse was replaced by a random number sampled from a Gaussian with its mean and SD being 740 min and 740 x 0.1 min, respectively, which were determined based on the empirical data.

(iii) Similarly, we replaced the data of the mutant group by random numbers sampled from a Gaussian, but its mean and SD (set to mean x 0.1 based on the F1/N2 male sleep data) were changed as variables.

(iv) For these surrogate data, we computed the LOD score using the *R/qtl* package in R. The procedures (i) – (iv) were repeated 10,000 times.

The simulation showed the LOD score as a function of the number of mice examined and of how far the mutant sleep parameter deviated from the

mean sleep parameter of the control mice (Figure 8A). Importantly, the simulation also showed moderate variability in the LOD score even under the same condition, which may be due to chance. One of the *Sleepy* pedigrees, B021, showed a LOD score of 32 for 118 N2 mice (Funato et al., 2016). The simulation predicted that a total wake time of a mutant pedigree showing a LOD score of 32 was approximately 500 min, which is indeed consistent with the sleep phenotype of *Sleepy* pedigrees (Figure 8A).

To confirm the causality of the gene mutation, we compare the sleep/wakefulness of mutant mice with control mice. We simulated the probability of reaching statistical significance ($P < 0.05$) in the two-sample *t*-test on the mean wake time of 10 control mice and 10 mutant mice. The mean wake time of each individual was randomly determined as described in the procedure (ii) above. The two-sample *t*-tests for 10,000 sets of randomly generated data was performed and the probability of reaching statistical significance is shown in Fig. 8B. The mutant group showing a mean daily wake time of approximately 650 min and 675 min showed 80% and 50% probability of reaching statistical significance ($p<0.05$), respectively. However, when we set the CV to 0.15, which can be found in the literature (Graves et al., 2003; Lee et al., 2004), the mutant mean wake time changed to 600 min (80% chance) and 640 min (50% chance), indicating the importance of highly consistent sleep measurements.

2.9 *Drowsy* pedigree carrying the *Cacna1a* mutation

The founder male of the B016 (*Drowsy*) pedigree had a total wake time of 502 min/24 h. Distribution of Drowsy N2 males deviated to short total wake time compared with unaffected mice (Figure 9A). QTL analysis showed a single LOD score peak of 5.17 for total wake time located around rs32729089 (chr8:74953357) and rs33601490 (chr8:91507617) (N = 81, Figure 9B). According to our simulation (data not shown), the total wake time of the pedigree showing a LOD score of 5.2 (N = 81) was expected to be 645-680 min, which was 60-95 min shorter than the wild-type group mean (740 min). Consistently, the difference in the total time between the *Drowsy* mutant group and the wild-type group was ~70 min.

Haplotype distribution of affected *Drowsy* N2 mice (total wake time in bottom 20%) was different from that of unaffected group (total wake time in top 20%) (Figure 9C). Whole-exome sequencing of the *Drowsy* pedigree identified a heterozygous single nucleotide substitution (chr8: 84461494) of the *Cacna1a* gene in 7 out of 8 Drowsy F1 mice with short total wake time (Figure 9E), and direct sequencing confirmed the nucleotide change (Figure 9D). CACNA1A is a voltage-dependent calcium channel that is highly expressed in cerebellar Purkinje cells and many other types of neurons (Rajakulendran et al., 2012). The mutation results in an amino acid substitution F102L in the first transmembrane region of domain I (Figure 9F), well-conserved among vertebrates and invertebrates (Figure 9G). Many

missense mutations in *Cacna1a* are associated with two autosomal dominant diseases, episodic ataxia type2 and familial hemiplegic migraine, as well as spinocerebellar ataxia 6 caused by a CAG repeat expansion in *Cacna1a* (Figure 9F) (Rajakulendran et al., 2012). As predicted, the homozygous *Drowsy* mutant suffered from severe abnormalities in locomotion and posture which was reported in *Cacna1a*-deficient mice (Fletcher et al., 2001; Jun et al., 1999). Notably, a recent computational simulation-based study showed the potential role of voltage-dependent calcium channel in sleep/wake maintenance (Tatsuki et al., 2016).

SECTION III: MATERIALS AND METHODS

Animals

All procedures were conducted in accordance with the Guidelines for Animal Experiments of University of Tsukuba and approved by the Institutional Animal Care and Use Committee of University of Tsukuba (Approved protocol ID #140200). B6J and B6N mice were obtained from CLEA Japan and Charles River. B10J mice were from The Jackson Laboratory (#000665). Mice were housed in a polysulfone cage (391 x 199 x 160 mm, floor area 501 cm^2, Techniplast #GM500) in individually ventilated cage racks (Techniplast #DGM70QX) under controlled conditions (12-h light/dark cycle, 23 ± 2°C, 55 ± 5% humidity, and *ad libitum* access to water and food). Mice were weaned at 4 weeks of age and housed in groups of up to 5 mice per cage.

In vitro fertilization

Sperms from mutagenized G0 mice were harvested at the age of 25-30 weeks and cryopreserved until use. To induce superovulation, adult female C57BL/6N mice were administered with pregnant mare serum gonadotropin followed by human chorionic gonadotropin (hCG) at 48-h intervals. Approximately 15-17 h after hCG treatment, we removed the oviducts from superovulated mice and collected the oocytes. The pooled oocytes obtained from 20 females were inseminated with capacitated sperm. After overnight culture, two-cell stage embryos were transferred into

pseudopregnant recipient females. To avoid overrepresentation of the same mutations in sperm differentiated from the same spermatogonia, 60 or fewer F1 males from a single G0 mouse were used for phenotypic screening.

EEG/EMG electrode and tether cable.

Each electrode is composed of an insulator (length 7.62 x width 6.08 x height 8.26 mm) with four metal pins (0.50 x 0.40 x 2.6 mm) that are 5.08 mm apart in the anteroposterior axis and 2.54 mm in the left-right axis. Two 15-mm-long Teflon-coated stainless wires (Cooner wire #AS633) extends from the center equidistance from the metal pins (Figure 10A). The Teflon-coat is removed 2 mm from the free end of the EMG wires and fused using lead-free solder. Four metal pins and EMG wires are gold-plated by immersing them in Supermex #250 (Metalor Technologies).

The electrode-end of a tether is composed of a 6-pin header (dissected from 2 x 40 pin header, Useconn Electronics Ltd., #PH-2x40SG) with the two outermost left-side pins for the EEG signals and two middle pins for the EMG signals (Figure 10B). The pin unit is covered with epoxy resin (Cemedine, High Super 30 #CA-193) or a heat-shrinkable tube (5 mm in diameter, black; Sumitomo Electric, SUMITUBE® C). The other end of the tether cable is composed of a slip ring (yosoo #yosoo-811-3, diameter 12.5mm) or cord detangler (Phillips #SJA4150/17), which allows the mouse to move freely in a recording cage. The electrode/tether unit is connected to a cable via 4-pin RJ11 plug that transmits signals to a preamplifier (Figure 10C).

EEG/EMG electrode implantation surgery

Eight- to ten-week-old mice (body weight >25 g) were subjected to EEG/EMG electrode implantation surgery. The surgery was performed under isoflurane anesthesia (4% for induction, 2% for maintenance). An incision was made on the scalp along the midline to expose the cranium. Four holes were made on the skull using 1.0-mm dental drill bits (anteroposterior: 0.50 mm, lateral: ±1.27 mm and anteroposterior: −4.53 mm, lateral: ±1.27 mm from bregma). The electrode pins were lowered onto the dura under stereotaxic control (David Kopf Instruments #940/926) and fixed using dental cement (3M ESPE, Ketac Cem Aplicap). Subsequently, two EMG wires were crossed once, inserted into the neck extensor muscles and covered with dental cement. The skins is , then, sutured to close the incision. A 6-pin header (dissected from 2 x 40 pin header, Useconn Electronics Ltd., #PH-2x40SG) was inserted into the top of the EEG/EMG electrode to close the holes of the insulator.

EEG/EMG Recording

Seven days after surgery, the mice were attached to a tether cable under isoflurane anesthesia, then single-housed in a recording cage (19.1 x 29.2 x 12.7 cm). The tether cable was hung by a counterbalanced lever arm (11.4 cm-long, Instech Laboratories #MCLA) that allows the mice to move freely. All mice were given at least 5 days of recovery from surgery and habituation

to the recording conditions for additional 4 days at the minimum. The floor of the cage was covered with aspen chips and nest materials. To examine sleep/wake behavior under baseline conditions, the EEG/EMG signal was recorded for three consecutive days from the onset of the light phase. Mice were deprived of sleep from ZT0 to ZT6 by intermittent mechanical agitation of the cages (Sinton et al., 2009) and subsequently recorded from ZT6 to ZT24 for 18-h.

EEG/EMG analysis

EEG/EMG signals were amplified, filtered (EEG: 0.3–300 Hz; EMG: 30–300 Hz) with a multi-channel amplifier (NIHON KODEN, #AB-611J), and digitized at a sampling rate of 250 Hz using an analogue-to-digital converter (National Instruments #PCI-6220) with LabVIEW software (National Instrument). The EEG/EMG data were visualized and semi-automatically analyzed by MATLAB-based software followed by visual inspection. Each 20-sec epoch was staged into wakefulness, NREM sleep and REM sleep. Wakefulness was scored based on the presence of low amplitude, fast EEG activity and high amplitude, variable EMG activity. NREM sleep was characterized by high amplitude, delta (1–4 Hz)-frequency EEG waves and a low EMG tonus, whereas REM sleep was staged based on theta (6–9 Hz)-dominant EEG oscillations and EMG atonia. The total time spent in wakefulness, NREM sleep, and REM sleep was summed as the total number of 20-s epochs in each state. Mean episode durations were determined by dividing the total time

spent in each state by the number of episodes of that state. Epochs that contained movement artifacts were included in the state totals but excluded from the subsequent spectral analysis. EEG signals were subjected to fast Fourier transform analysis from 1 to 30 Hz with 1-Hz bins using MATLAB-based custom software. The EEG power density in each frequency bin was normalized to the sum of 16-30 Hz in all sleep/wake state.

Linkage analysis using SNPs between C57BL/6J and C57BL/6N

We sequenced SNPs of C57BL/6JJcl, C57BL/6NJcl, C57BL/6NCrl, and C57BL/6NCrlCrlj to select 96 SNPs of C57BL/6JJcl that differ from C57BL/6NJcl, C57BL/6NCrl and C57BL/6NCrlCrlj (Table 1, Figure 2) (Kumar et al., 2013). DNA was purified from tails of mice using a Qiagen kit (DNeasy Blood & Tissue Kit, QIAGEN #69504). SNPs between C57BL/6J and C57BL/6N of N2 mice were determined using a custom TaqMan Genotyping assay (Thermo Fisher). The QTL analysis was performed using R/qtl software (version 1.42-8; www.rqtl.org) (Broman et al., 2003).

Whole-exome sequencing

Exome sequencing libraries were prepared with the SeqCap EZ Developer Library kit (MM10 exome, cat# 110624, Roche NimbleGen) from 500 ng of genomic DNA to determine the number of mutations in the mutagenized mice. Sequencing of the multiplexed library using the 151x2 paired-end mode in the NextSeq 500 sequencer (Illumina) was performed by i-

Laboratory LLP sequencing service (Tsukuba, Japan). Reads in FASTQ files were imported into the CLC Genomics Workbench (Qiagen), trimmed by 1-base at the 3' end, and mapped to the mm10 mouse reference, which represents the C57BL/6J strain genome. Exome sequencing statistics were calculated to capture the target region definition provided by the SeqCap kit. Variant calls were performed using the Basic Variant Detection tool. Potential variants were filtered against control mouse variants. Nonsynonymous base substitutions and small InDels were identified based on ENSEMBLE transcript annotation.

For the B016 pedigree, whole exomes were captured with SureSelectXT2 Mouse All Exon (Agilent) and processed to a paired-end 2 x 100-bp run on the Illumina HiSeq2000 platform at the University of Texas Southwestern Medical Center, Next Generation Sequencing Core. Reads were mapped to the University of California Santa Cruz mm9 genome reference sequence for C57BL/6J using Burrows-Wheeler Aligner and quality filtered using SAMtools. Cleaned BAM files were used to realign the data and call variants using the Genome Analysis Tool Kit to detect heterozygous mutations.

Genotyping

To detect a single nucleotide change as routine genotyping, we used the dCAPS method in which PCR products are digested by restriction enzymes (Neff et al., 2002). dCAPS Finder (http://helix.wustl.edu/dcaps/dcaps.html) was used to design the primers.

Statistics

Statistical analysis was performed using SPSS Statistics 22 (IBM) and R software. All data were tested for a Gaussian distribution and variance. We used one-way analysis of variance (ANOVA) followed by Tukey's test to assess sleep parameters of mouse substrains. To assess the reproducibility of the sleep parameters, data from the first and second recordings were analyzed using Pearson's correlation test. $P < 0.05$ was considered statistically significant.

SECTION IV: CONCLUSION

We described the method for EEG/EMG-based sleep screening of randomly mutagenized mice and discussed the selection of inbred mouse strains. Statistically examined reproducibility of the selected screening parameters proved the precision of the sleep/wake measurement. Furthermore, we showed the workflow for identifying the causative gene; as an example, the identification of a *Cacna1a* mutation in the Drowsy pedigree showing a mild hypersomnia phenotype.

At the scale of ~10,000 mice, we identified 10 heritable loci to date. While low occurrence of sleep phenodeviant was expected, possibly due to redundant regulatory mechanisms in sleep/wakefulness and low penetrance of the phenotype, our screening output seems to be comparable to other trials where a single biological trait is screened (Vitaterna et al., 2006). The Clock ENU mutant is a lucky example that found the causal mutation from screening 304 G1 progeny (Vitaterna et al., 1994). Daxinger *et al.* reported identification of a single candidate gene from a population of 2,045 G1 mice (Daxinger et al., 2013). Another study showed 20 mutant progeny that carry 10 unique gene mutations from screening of approximately 5,000 G1 offspring, of which 9 were previously known genes in epigenetic regulation (Furuse et al., 2010).

The identified genes in our study usually encode proteins with large molecular weights, probably because the cumulative frequency of ENU-induced mutation is proportional to the gene size (Bauer et al., 2015); some of known sleep regulatory genes, such as the very compact orexin and orexin receptor genes, have not been detected in this screening. Also, for unknown reasons, the majority of our sleep phenodeviants has been long-sleep mutants.

Phenotype-driven screening at such large scale, indeed, is labor-intensive and costly. It is not recommended for an attempt to furthering the knowledge of largely defined mechanisms since there is a high chance of identifying already known genes, as it was the case of our obesity screening (Hossain et al., 2016). Also, in a dominant screening we recommend a highly focused screen rather than trying to examine multiple biological traits in a workflow; after all, the most expensive step in the screening is phenotyping, not the production of mutagenized mice. It is difficult to draw estimation on further identification of candidate genes and whether/when saturation can be reached in a dominant screen (Nolan et al., 1997). Nevertheless, we should find more genes in sleep/wake regulation by enlarging the scale and continuing the search. The screening strategy is easily modifiable for studying other physiological phenomena in mice with careful selection of the screening criteria and the biology to be studied.

SECTION V: FIGURES AND TABLES

Figure 1 Phylogenetic tree of C57BL substrains

Abbreviations for the substrain genealogy: N, National Institutes of Health; J, Jackson Laboratory; Crl, Charles River Laboratories; Crlj, Charles River Laboratories Japan; Jcl, CLEA Japan. (Jackson Laboratory, https://www.jax.org)

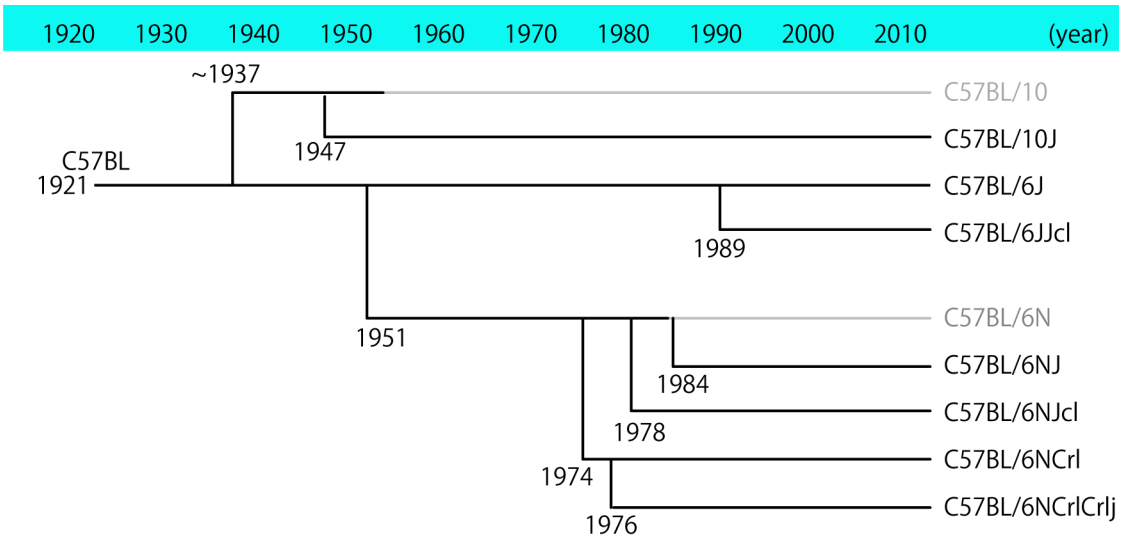

Figure 2 Chromosomal location of SNPs for linkage analysis

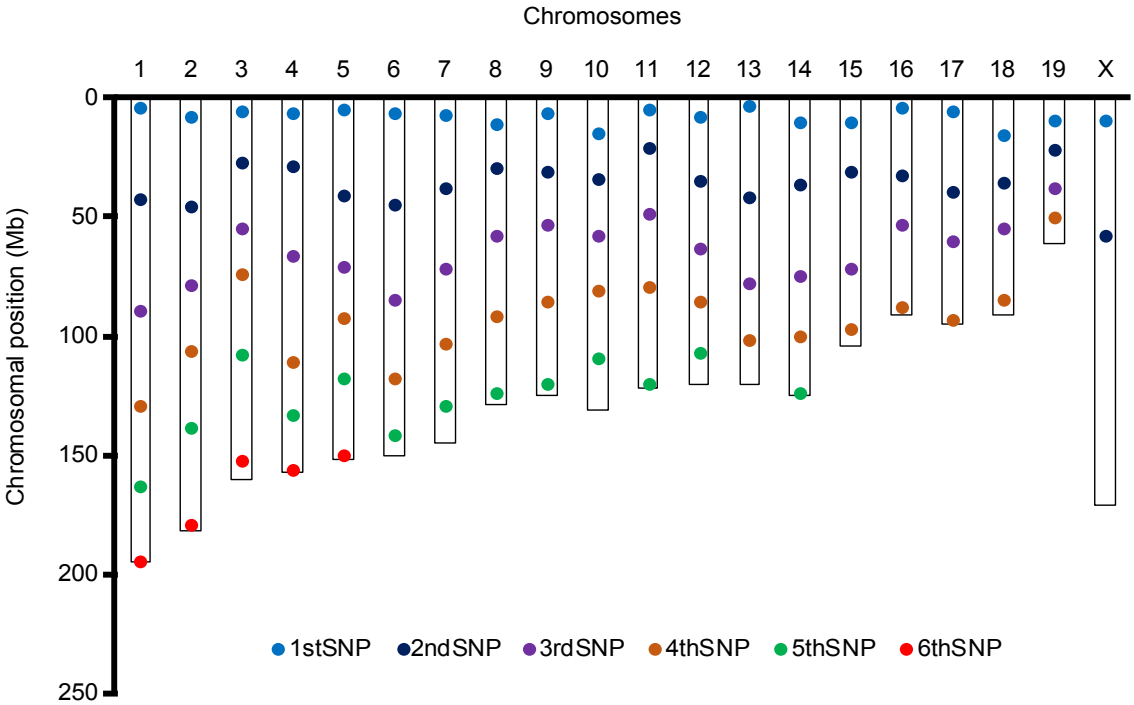

Figure 3 Sleep parameters in B6J, B6N and B10J.
Total time spent in (A) wake (B) NREMS and (C) REMS. Episode duration during (D) wake, (E) NREMS and (F) REMS. EEG power spectrum during (G) NREMS and (H) REMS. (I) The delta density (1-4 Hz) during NREMS and (J) the theta density (6-9 Hz) during REMS. Male B6J (N = 21), B6N (N = 20) and B10J (N = 20). All data are shown as the mean ± SEM **P* < 0.05; ***P* < 0.01; ****P* < 0.001; *****P* < 0.0001. Two-way ANOVA followed by Tukey's test (A-H). One-way ANOVA followed by Tukey's test (I, J)

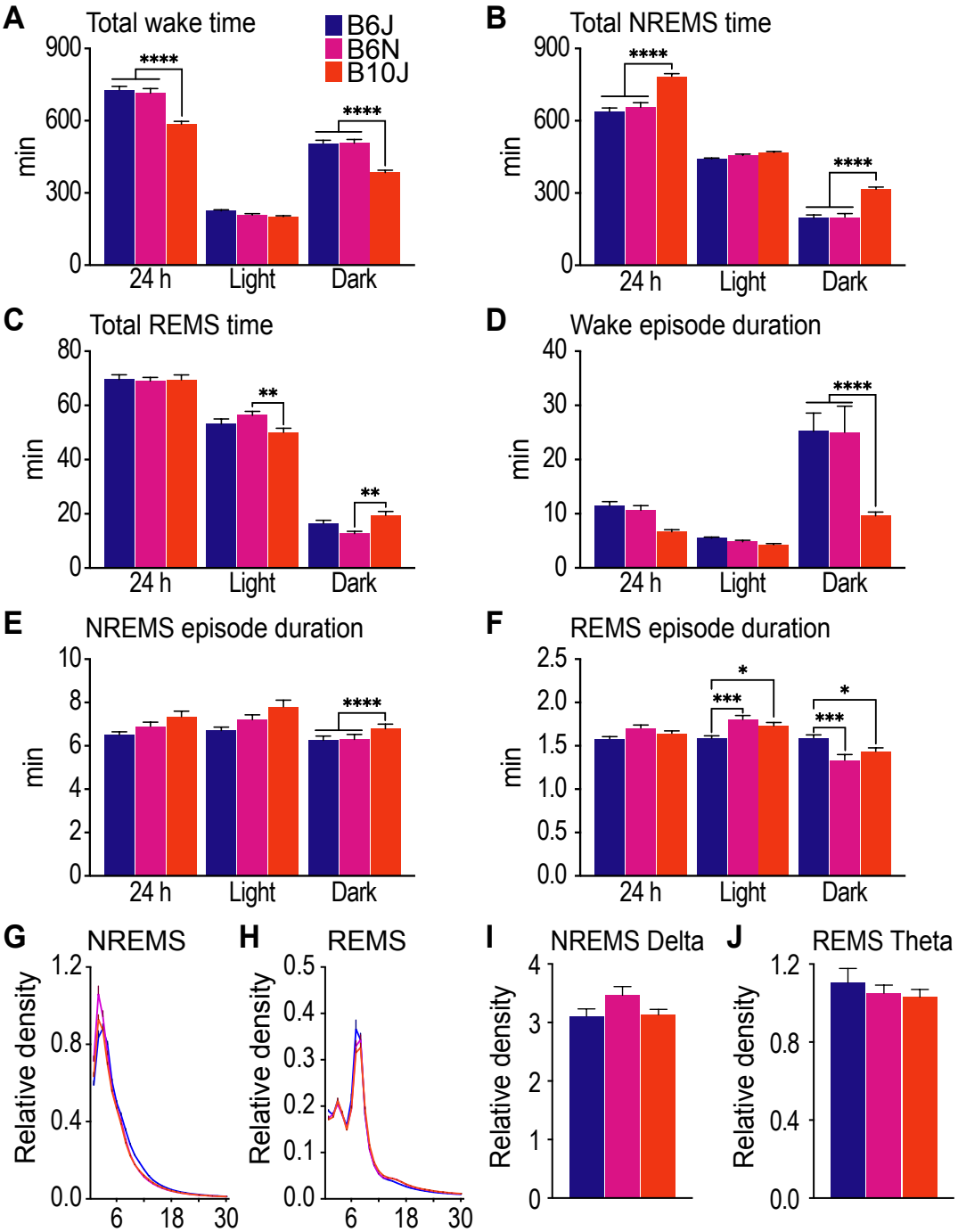

Figure 4 Recovery sleep after 6-h sleep deprivation.
(A) Wake, (B) NREMS, (C) REMS during 18-h recovery following 6-h sleep deprivation. (D) NREMS EEG delta decay during the 18-h recovery. Recovery delta power is normalized by the last hour of the light phase (ZT11) of the baseline. Red-filled box, 6-h sleep deprivation; white box, 6-h recovery sleep; gray-filled box, 12-h dark phase. (E) Change, shown as ratio (recovery/baseline), in time spent in each vigilance state during dark phase (ZT12-ZT24). Male B6J (N = 19), B6N (N = 18) and B10J (N = 20). All data are shown as the mean ± SEM *P < 0.05; ** (blue) P < 0.01; *** (green) P < 0.001; **** (red) P < 0.0001. Two-way ANOVA followed by Tukey's test.

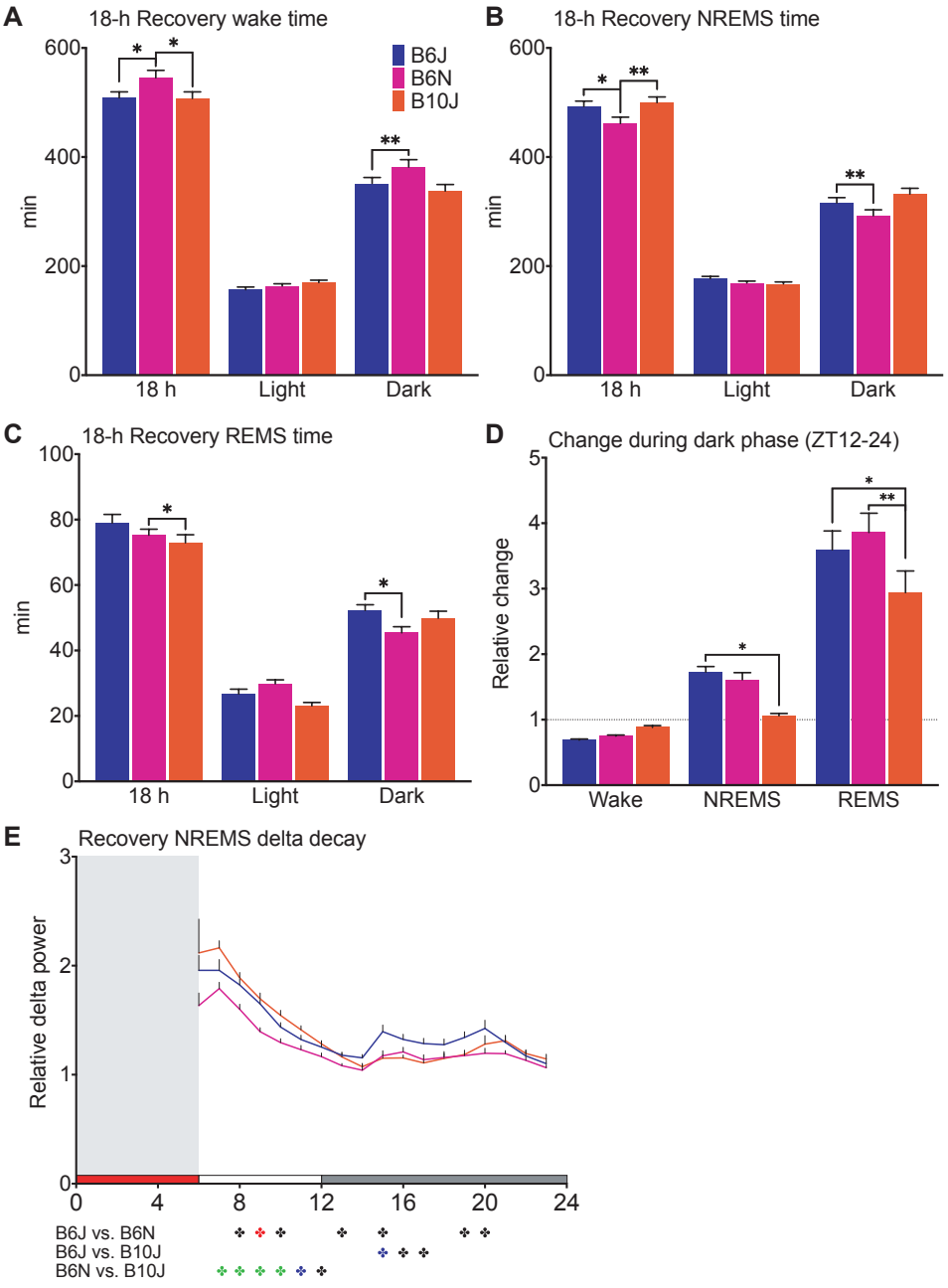

Figure 5 Screening strategy in sleep and wake behavior

(A) Recessive screening scheme. In an intercross scheme (shaded), a sibling mating between heterozygous G2 male and female is used to produce G3 generation. In a backcross scheme (dotted), G1 founder is crossed with G2 mutant daughter. (B) In the dominant screening, each F1 phenodeviant is crossed with female wild-type B6N mice to obtain N2 mice. Male N2 mice are examined whether the sleep abnormality is heritable. If heritability is confirmed, N2 mice are used for QTL analysis and whole-exome sequencing to identify the gene mutation associated with the sleep phenotype. (C) Examples of heritability test results. Phenodeviant A: normal sleep phenotype; sleep parameter histogram in N2 mice showing similar trend as the normal population (+/+, green). Phenodeviant B: subtle sleep phenotype, heritability cannot be determined (*?*/+, yellow). Phenodeviant C: heritable and weak sleep phenotype. Many N2 mice (*?* /+) cannot be determined as either phenodeviant (*m*/+) or normal (+/+) based on the sleep behavior. Phenodeviant D: heritable and strong sleep phenotype. Each N2 mouse can be assigned as either phenodeviant (*m*/+) or normal (+/+).

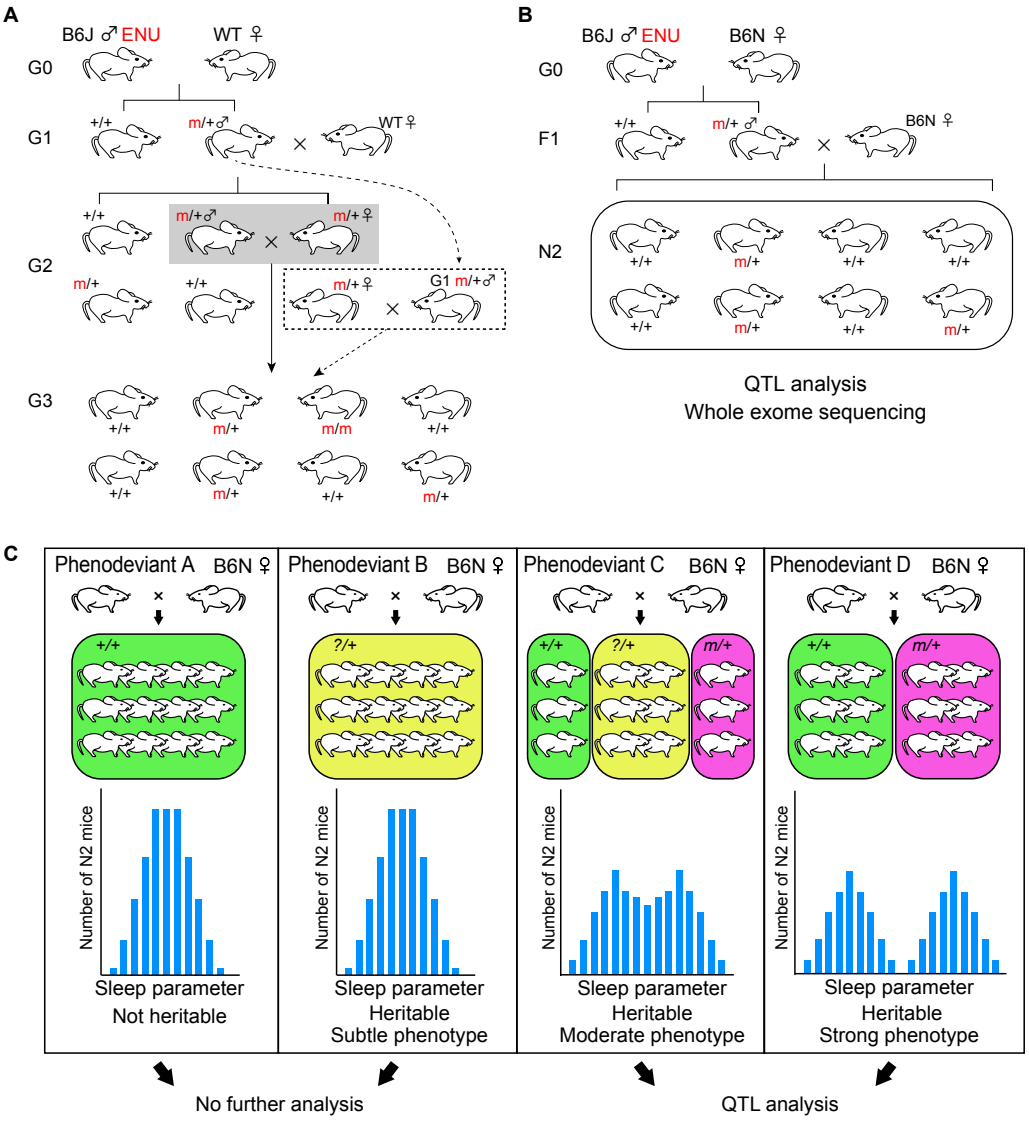

Figure 6 Number of non-overlapped mutations
The expected number of non-overlapped F1 mutant mice derived from a single G0 mouse for N_{sp}=70, when three ENU treatments killed 99.9% of stem-cell-like spermatogonia (red curve). For reference, the results for N_{sp} = 70,000 (when all stem-cell-like spermatogonia in two testes survived the ENU treatments) is also shown (blue line).

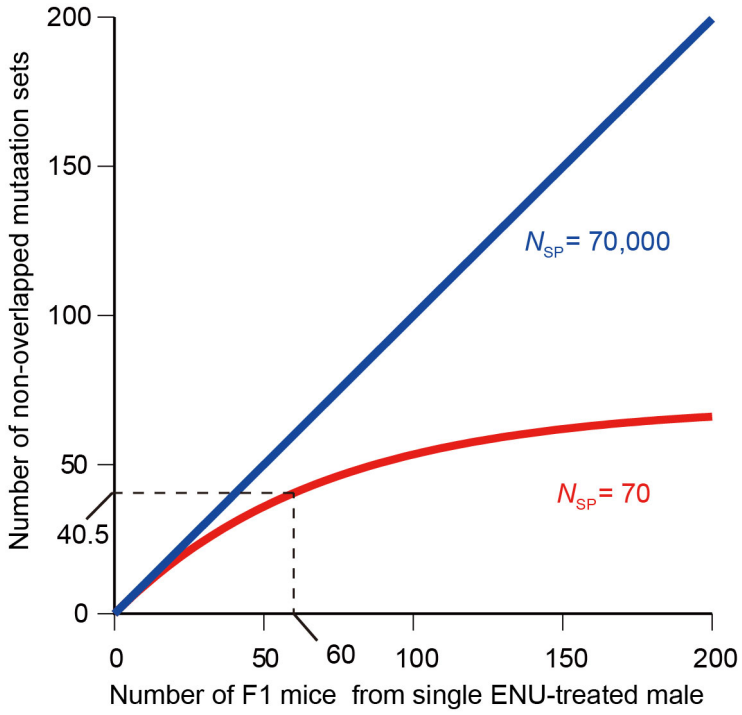

Figure 7 Reproducibility of the sleep parameters

Reproducibility of sleep parameters between basal recording (1st) and second recording (2nd). Total time in (A) wake, (B) NREMS and (C) REMS. Episode duration of (D) wake, (E) NREMS, and (F) REMS. Total time during 18 h after 6-h sleep deprivation in (G) wake and (H*)* NREMS. (I) Delta Density (1-4 Hz) during NREMS and (H) theta density (6-9 Hz) during REMS. B6N (N = 37). Each line indicates a regression line. Pearson's correlation coefficient (r) and probability (P) are indicated.

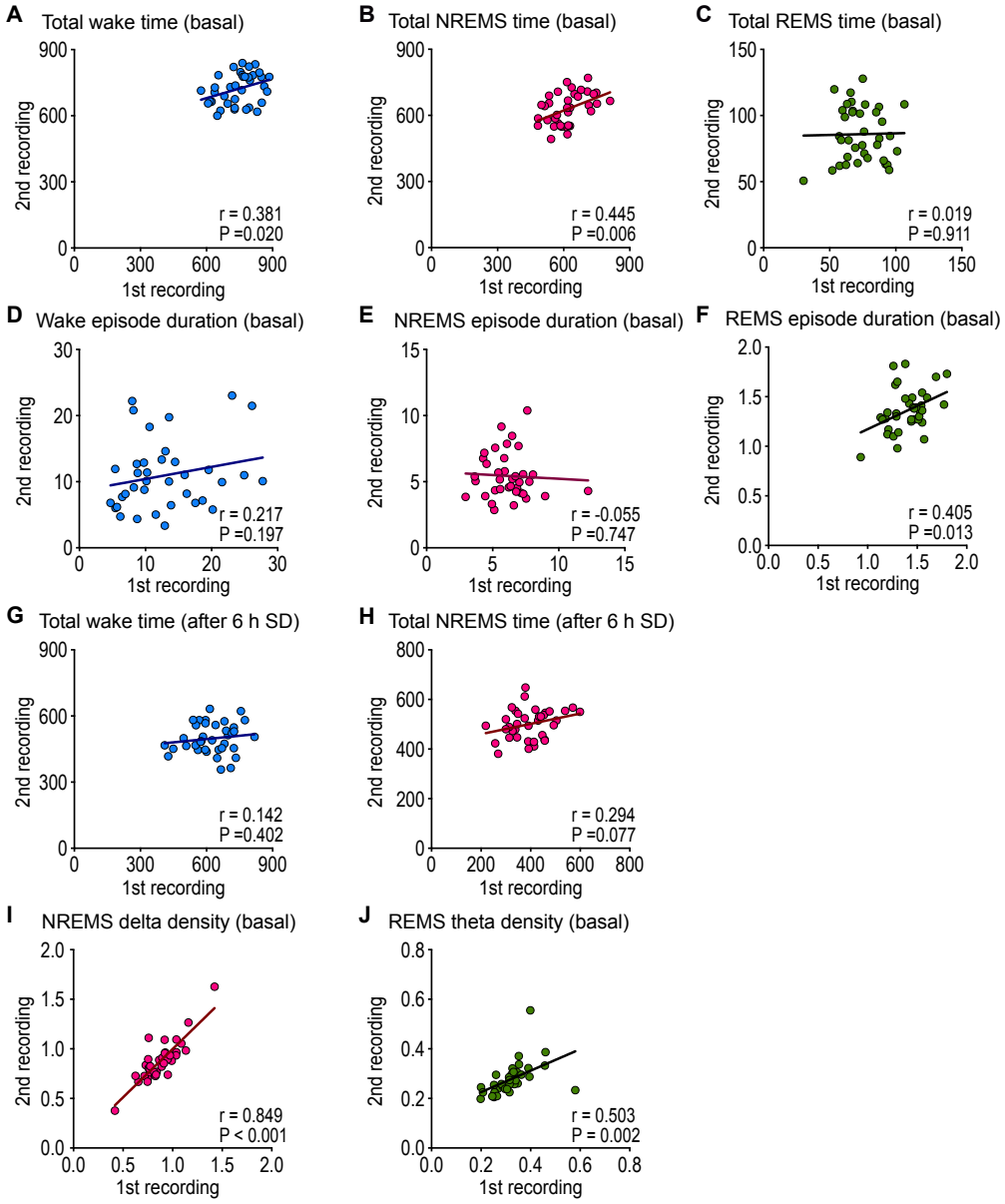

Figure 8 Simulation of statistical tests.
(A) The LOD score computed for surrogate data with various mean wake time of the mutant group of 60 (blue), and 120 (red) N2 mice. The lines and shaded areas indicate the averages and 95% confidence intervals of the obtained LOD score calculated based on 10,000 sets of surrogate data, respectively. In each case, we assumed that 50% of population were mutants. The black square in panel (A) indicates the *Sleepy* mutant pedigree, B021. (B) The probability of reaching statistical significance in a two-sample *t*-test on the mean wake time of 10 control and 10 mutant mice. The results were averaged over 10,000 trials.

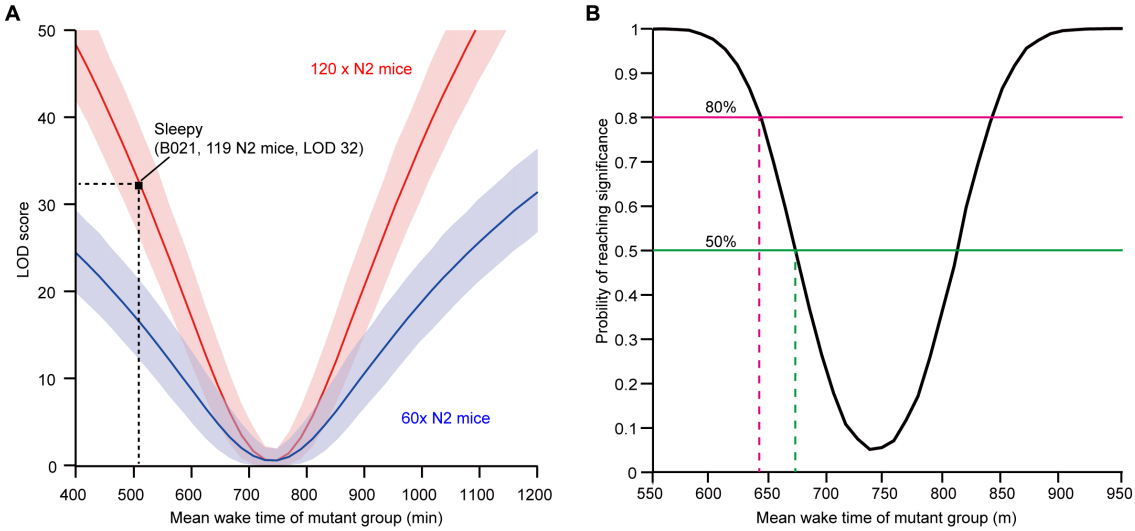

Figure 9 Identification of the *Cacna1a* gene mutation in the *Drowsy* pedigree

(A) Wake time distribution of retrospectively genotyped Drowsy N2 littermates. *Cacna1a*$^{+/+}$ (blue) and *Cacna1a*$^{m/+}$ (red) mice. (B) QTL analysis of the Drowsy pedigree for total wake time (N = 81). (Inset) LOD score peak between rs13479672 and rs33601490 on chromosome 8. (C) Haplotype analysis of Drowsy mutant pedigrees with sleepy phenotypes (bottom 20% in total wake time) and without a sleepy phenotype (top 20% in total wake time). (D) Direct sequencing of the *Cacna1a* gene in *Cacna1a*$^{+/+}$, *Cacna1a*$^{m/+}$ and *Cacna1a*$^{m/m}$ mice. (E) Mutational analysis of affected mice (bottom 20% in total wake time) and unaffected mice (top 20% in total wake time) within the Drowsy pedigree. (F) Structures of the CACNA1A protein indicating the current F102L mutation and selected human missense mutations reported in familial hemiplegic migraine (yellow) and episodic ataxia type2 (green) and polyglutamine in spinocerebellar ataxia type 6 (Gln). (G) Phylogenetic conservation around phenylalanine 102.

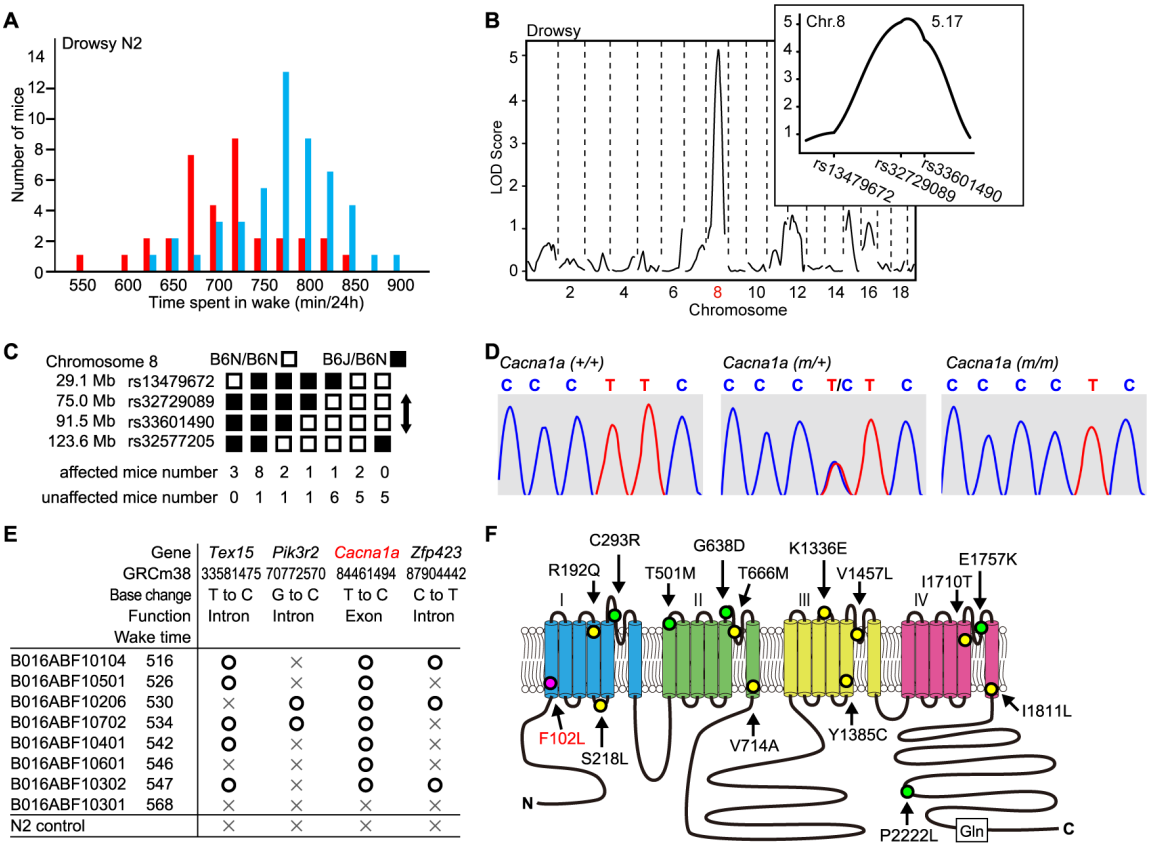

Figure 10 Design of the electrode and cables.
(A) Bottom, side and front views of an electrode for EEG and EMG. Four EEG electrodes and one end of two EMG wires are gold-plated. Two of four EEG electrodes are actually used to obtain the EEG signal. Four protrusions close to each EEG electrode enable fixation of the position of an electrode at a certain depth during implantation surgery. The unit for measurements is millimeters. (B) A tether cable connects an EEG/EMG electrode and a cable that is connected to a preamp. The top of the tether cable is composed of a 4-pin detangler. (C) A cable transmits EEG/EMG signal from the tether cable to a preamp.

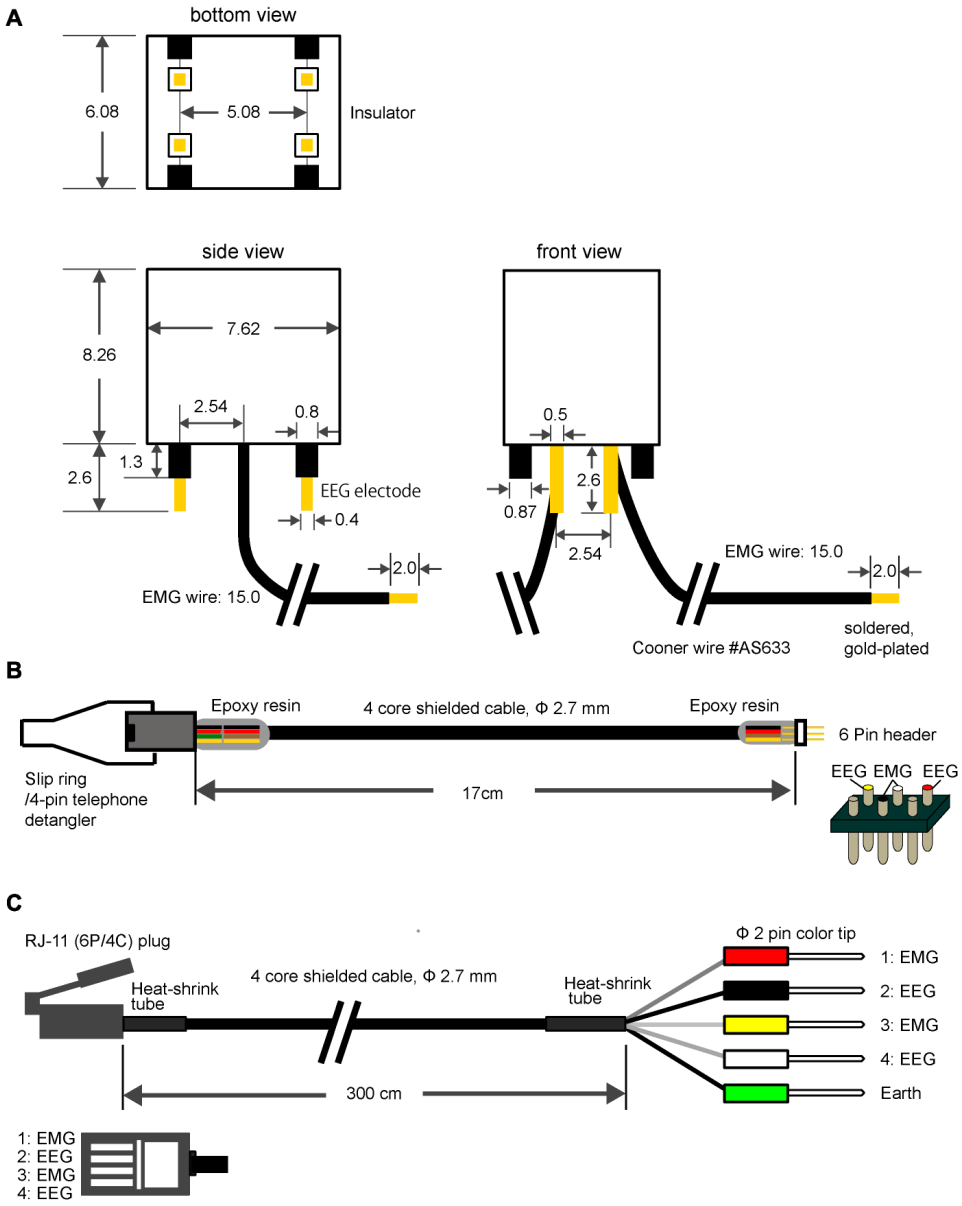

Table 2. SNP list for linkage analysis of C57BL/6J and C57BL/6N substrains

Chromosome	Position(mm10)	rs number	B6J	B6N
Chr1	1:3607559	rs32685032	A	T
Chr1	1:42367595	rs31362610	T	C
Chr1	1:88806692	rs242608911	C	T
Chr1	1:129386361	rs6327099	T	C
Chr1	1:163132699	rs6341208	A	T
Chr1	1:194246275	rs242712390	C	A
Chr2	2:8069855	rs13476337	A	T
Chr2	2:45143008	rs33488914	A	G
Chr2	2:78799176	rs33162749	C	T
Chr2	2:106074143	rs227312316	G	A
Chr2	2:138480020	rs13476801	T	C
Chr2	2:179262364	rs29673978	T	C
Chr3	3:5370727	rs13476956	C	T
Chr3	3:27240831	rs237712466	T	G
Chr3	3:54425630	rs31338752	A	G
Chr3	3:74118533	rs31154737	A	T
Chr3	3:107470377	rs31321678	A	G
Chr3	3:152219576	rs31594267	A	C
Chr4	4:6374701	rs32143059	G	A
Chr4	4:28322410	rs13477622	T	C
Chr4	4:65944235	rs13477746	T	C
Chr4	4:110650398	rs245725397	C	T
Chr4	4:132595336	rs46988409	C	A
Chr4	4:155910817	rs6397070	T	C
Chr5	5:4547791	rs247844351	C	T
Chr5	5:40761789	rs33508711	C	T
Chr5	5:70742061	rs13478320	C	A
Chr5	5:92081078	rs33249065	A	G
Chr5	5:117459347	rs3662161	A	G
Chr5	5:149626021	rs33208334	T	C
Chr6	6:6233941	rs30450019	A	G
Chr6	6:44286336	rs30892442	A	C
Chr6	6:80305689	rs48566826	T	A
Chr6	6:117470880	rs13478995	C	G
Chr6	6:141072590	rs235068709	G	T
Chr7	7:6976737	rs242748489	G	A
Chr7	7:37431938	rs31221380	A	C
Chr7	7:71816909	rs32060039	C	G
Chr7	7:104047611	rs46252790	G	A
Chr7	7:129035694	rs13479522	A	G
Chr8	8:10521755	rs13479605	C	A
Chr8	8:29097075	rs13479672	T	C
Chr8	chr8:56318886	rs32785829	A	G
Chr8	8:91507617	rs33601490	T	C
Chr8	8:123630996	rs32577205	A	G
Chr9	9:6238770	rs33672596	A	G
Chr9	9:31156626	rs13480122	T	C
Chr9	9:52785119	rs29644859	T	G
Chr9	9:85239185	rs260373537	T	C
Chr9	9:119641498	rs30431245	T	C
Chr10	10:5030776	rs50477269	A	G
Chr10	10:33653023	rs13480575	T	C
Chr10	10:57752462	rs13480619	T	C
Chr10	10:80795365	rs13459122	A	T
Chr10	10:109378627	rs13480759	C	T

Chr11	11:4508730	rs3659787	G	A
Chr11	11:21140133	rs29413390	A	G
Chr11	11:48117382	rs13481014	T	C
Chr11	11:79252230	rs13481117	G	T
Chr11	11:120306788	rs49027247	T	C
Chr12	12:7453718	rs29142759	A	G
Chr12	12:34467966	rs29487143	G	C
Chr12	12:62767534	rs29133146	A	C
Chr12	12:85645337	rs13481569	G	A
Chr12	12:106833655	rs13481634	A	C
Chr13	13:18724094	rs29242536	A	G
Chr13	13:41442786	rs3722313	T	C
Chr13	13:77411106	rs29802434	G	C
Chr13	13:101209232	rs3702296	A	G
Chr14	14:9937385	rs31187642	G	A
Chr14	14:36479449	rs31133670	A	G
Chr14	14:74415721	rs30264676	T	A
Chr14	14:99624996	rs31059846	A	G
Chr14	14:124108797	rs31233932	C	T
Chr15	15:9757093	rs257670740	T	C
Chr15	15:30613567	rs261563123	C	T
Chr15	15:71632551	rs31858887	T	C
Chr15	15:97255365	rs31921278	A	G
Chr16	16:4238020	rs4152511	T	C
Chr16	chr16:32451615	rs257082658	T	G
Chr16	16:52739944	rs4187179	T	C
Chr16	16:87819629	rs4214728	T	C
Chr17	17:5332903	rs4137196	T	C
Chr17	17:39170355	rs33334258	G	A
Chr17	17:60319945	rs13483055	T	C
Chr17	17:93830797	rs33132419	T	C
Chr18	18:15249748	rs13483221	C	T
Chr18	18:35206506	rs13483296	A	T
Chr18	18:54614841	rs13483369	A	C
Chr18	18:84516845	rs29690544	T	C
Chr19	19:9027005	rs31112038	G	C
Chr19	19:21913323	rs45985634	A	T
Chr19	19:38005411	rs30953636	G	T
Chr19	19:49976154	rs3724876	G	T
Chr.20 (X)	X:17562057	rs31353361	T	C
Chr.20 (X)	X:57867627	rs6368704	A	G

BIBLIOGRAPHY

Bauer, D.C., McMorran, B.J., Foote, S.J., and Burgio, G. (2015). Genome-wide analysis of chemically induced mutations in mouse in phenotype-driven screens. BMC Genomics *16*, 866.

Beutler, B., Du, X., and Xia, Y. (2007). Precis on forward genetics in mice. Nat. Immunol. *8*, 659–664.

Broman, K.W., Wu, H., Sen, Ś., and Churchill, G.A. (2003). R/qtl: QTL mapping in experimental crosses. Bioinformatics *19*, 889–890.

Chemelli, R.M., Willie, J.T., Sinton, C.M., Elmquist, J.K., Scammell, T.E., Lee, C., Richardson, J.A., Williams, S.C., Xiong, Y., Kisanuki, Y., et al. (1999). Narcolepsy in orexin knockout mice: Molecular genetics of sleep regulation. Cell *98*, 437–451.

Chinwalla, A.T., Cook, L.L., Delehaunty, K.D., Fewell, G.A., Fulton, L.A., Fulton, R.S., Graves, T.A., Hillier, L.W., Mardis, E.R., McPherson, J.D., et al. (2002). Initial sequencing and comparative analysis of the mouse genome. Nature *420*, 520–562.

Citri, Y., Colot, H. V, Jacquier, A.C., Yu, Q., Hall, J.C., Baltimore, D., and Rosbash, M. (1987). A family of unusually spliced biologically active transcripts encoded by a Drosophila clock gene. Nature *326*, 42–47.

Coleman, P.J., Gotter, A.L., Herring, W.J., Winrow, C.J., and Renger, J.J. (2017). The Discovery of Suvorexant, the First Orexin Receptor Drug for Insomnia. Annu. Rev. Pharmacol. Toxicol. *57*, 509–533.

Daxinger, L., Harten, S.K., Oey, H., Epp, T., Isbel, L., Huang, E., Whitelaw, N., Apedaile, A., Sorolla, A., Yong, J., et al. (2013). An ENU mutagenesis screen identifies novel and known genes involved in epigenetic processes in the mouse. Genome Biol. *14*.

DeBruyne, J.P., Noton, E., Lambert, C.M., Maywood, E.S., Weaver, D.R., and Reppert, S.M. (2006). A Clock Shock: Mouse CLOCK Is Not Required for Circadian Oscillator Function. Neuron *50*, 465–477.

Fletcher, C., Tottene, A., Lennon, V., Wilson, S., Dubel, S., Paylor, R., Hosford, D., Tessarollo, L., McEnery, M., Pietrobon, D., et al. (2001). Dystonia and cerebellar atrophy in Cacna1a null mice lacking P/Q calcium channel activity. FASEB J. *15*, 1288–1290.

Franken, P., Malafosse, A., and Tafti, M. (1998). Genetic variation in EEG activity during sleep in inbred mice. AJP - Regul. Integr. Comp. Physiol. *275*, R1127–R1137.

Franken, P., Chollet, D., and Tafti, M. (2001). The Homeostatic Regulation of Sleep Need Is under Genetic Control. J. Neurosci. *21*, 2610–2621.

Funato, H., Miyoshi, C., Fujiyama, T., Kanda, T., Sato, M., Wang, Z., Ma, J., Nakane, S., Tomita, J., Ikkyu, A., et al. (2016). Forward-genetics analysis of sleep in randomly mutagenized mice. Nature *539*, 378–383.

Furuse, T., Wada, Y., Hattori, K., Yamada, I., Kushida, T., Shibukawa, Y., Masuya, H., Kaneda, H., Miura, I., Seno, N., et al. (2010). Phenotypic characterization of a new Grin1 mutant mouse generated by ENU mutagenesis. Eur. J. Neurosci. *31*, 1281–1291.

Goel, N. (2017). Genetic Markers of Sleep and Sleepiness. Sleep Med. Clin. *12*, 289–299.

Goldowitz, D., Frankel, W.N., Takahashi, J.S., Holtz-Vitaterna, M., Bult, C., Kibbe, W. a., Snoddy, J., Li, Y., Pretel, S., Yates, J., et al. (2004). Large-scale mutagenesis of the mouse to understand the genetic bases of nervous system structure and function. In Molecular Brain Research, (Elsevier), pp. 105–115.

Graves, L.A., Hellman, K., Veasey, S., Blendy, J.A., Pack, A.I., and Abel, T. (2003). Genetic Evidence for a Role of CREB in Sustained Cortical Arousal. J. Neurophysiol. *90*, 1152–1159.

Hayasaka, N., Hirano, A., Miyoshi, Y., Tokuda, I.T., Yoshitane, H., Matsuda, J., and Fukada, Y. (2017). Salt-inducible kinase 3 regulates the mammalian circadian clock by destabilizing PER2 protein. Elife *6*, 1–17.

Hendricks, J.C., Finn, S.M., Panckeri, K.A., Chavkin, J., Williams, J.A., Sehgal, A., and Pack, A.I. (2000). Rest in Drosophila Is a Sleep-like State. Neuron *25*, 129–138.

Hitotsumachi, S., Carpenter, D.A., and Russell, W.L. (1985). Dose-repetition increases the mutagenic effectiveness of N-ethyl-N-nitrosourea in mouse spermatogonia. Proc. Natl. Acad. Sci. *82*, 6619–6621.

Hossain, M.S., Asano, F., Fujiyama, T., Miyoshi, C., Sato, M., Ikkyu, A., Kanno, S., Hotta, N., Kakizaki, M., Honda, T., et al. (2016). Identification of mutations through dominant screening for obesity using C57BL/6 substrains. Sci. Rep. *6*, 32453.

Jun, K., Piedras-Renteria, E.S., Smith, S.M., Wheeler, D.B., Lee, S.B., Lee, T.G., Chin, H., Adams, M.E., Scheller, R.H., Tsien, R.W., et al. (1999). Ablation of P/Q-type Ca2+ channel currents, altered synaptic transmission, and progressive ataxia in mice lacking the alpha 1A-subunit. Proc. Natl. Acad. Sci. *96*, 15245–15250.

King, D.P., Zhao, Y., Sangoram, A.M., Wilsbacher, L.D., Tanaka, M., Antoch, M.P., Steeves, T.D.L., Vitaterna, M.H., Kornhauser, J.M., Lowrey, P.L., et al. (1997). Positional Cloning of the Mouse Circadian Clock Gene. Cell *89*, 641–653.

Komiya, H., Miyoshi, C., Iwasaki, K., Hotta-Hirashima, N., Ikkyu, A., Kanno, S., Honda, T., Gosho, M., Hamada, H., Satoh, T., et al. (2018). Sleep/Wake Behaviors in Mice During Pregnancy and Pregnancy-Associated Hypertensive Mice. Sleep *41*, 1–14.

Konopka, R.J., and Benzer, S. (1971). Clock Mutants of Drosophila melanogaster. Proc. Natl. Acad. Sci. *68*, 2112–2116.

Kumar, V., Kim, K., Joseph, C., Kourrich, S., Yoo, S.-H., Huang, H.C., Vitaterna, M.H., Pardo-Manuel de Villena, F., Churchill, G., Bonci, A., et al. (2013). C57BL/6N Mutation in Cytoplasmic FMRP interacting protein 2 Regulates Cocaine Response. Science *342*, 1508–1512.

Lee, J., Kim, D., and Shin, H.-S. (2004). Lack of delta waves and sleep disturbances during non-rapid eye movement sleep in mice lacking 1G-subunit of T-type calcium channels. Proc. Natl. Acad. Sci. *101*, 18195–18199.

Mekada, K., Hirose, M., Murakami, A., and Yoshiki, A. (2015). Development of SNP markers for C57BL/6N-derived mouse inbred strains. Exp. Anim. *64*, 91–100.

Neff, M.M., Turk, E., and Kalishman, M. (2002). Web-based primer design for single nucleotide polymorphism analysis. Trends Genet. *18*, 613–615.

Nelson, A., Faraguna, U., Zoltan, J., Tononi, G., and Cirelli, C. (2013). Sleep Patterns and Homeostatic Mechanisms in Adolescent Mice. Brain Sci. *3*, 318–343.

Nolan, P.M., Kapfhamer, D., and Bućan, M. (1997). Random Mutagenesis Screen for Dominant Behavioral Mutations in Mice. Methods *13*, 379–395.

Oakberg, E.F., and Crosthwait, C.D. (1983). The effect of ethyl-, methyl- and hydroxyethyl-nitrosourea on the mouse testis. Mutat. Res. Mol. Mech. Mutagen. *108*, 337–344.

van Ooijen, J.W. (1999). LOD significance thresholds for QTL analysis in experimental populations of diploid species. Heredity (Edinb). *83*, 613–624.

Rajakulendran, S., Kaski, D., and Hanna, M.G. (2012). Neuronal P/Q-type calcium channel dysfunction in inherited disorders of the CNS. Nat. Rev. Neurol. *8*, 86–96.

Reddy, P., Zehring, W.A., Wheeler, D.A., Pirrotta, V., Hadfield, C., Hall, J.C., and Rosbash, M. (1984). Molecular analysis of the period locus in Drosophila melanogaster and identification of a transcript involved in biological rhythms. Cell *38*, 701–710.

Ripperger, J.A., Jud, C., and Albrecht, U. (2011). The daily rhythm of mice. FEBS Lett. *585*, 1384–1392.

Russell, W.L., Kelly, E.M., Hunsicker, P.R., Bangham, J.W., Maddux, S.C., and Phipps, E.L. (1979). Specific-locus test shows ethylnitrosourea to be the most potent mutagen in the mouse. Proc. Natl. Acad. Sci. *76*, 5818–5819.

Shaw, P.J. (2000). Correlates of Sleep and Waking in Drosophila melanogaster. Science *287*, 1834–1837.

Shi, G., Wu, D., Ptáček, L.J., and Fu, Y.-H.H. (2017). Human genetics and sleep behavior. Curr. Opin. Neurobiol. *44*, 43–49.

Siepka, S.M., and Takahashi, J.S. (2005). Methods to record circadian rhythm wheel running activity in mice. Methods Enzymol. *393*, 230–239.

Simon, M.M., Moresco, E.M.Y., Bull, K.R., Kumar, S., Mallon, A.-M., Beutler, B., and Potter, P.K. (2015). Current strategies for mutation detection in phenotype-driven screens utilising next generation sequencing. Mamm. Genome *26*, 486–500.

Sinton, C.M., Kovakkattu, D., and Friese, R.S. (2009). Validation of a novel method to interrupt sleep in the mouse. J. Neurosci. Methods *184*, 71–78.

Tafti, Chollet, Valatx, and Franken (1999). Quantitative trait loci approach to the genetics of sleep in recombinant inbred mice. J. Sleep Res. *8*, 37–43.

Tagelenbosch, R.A.J., and de Rooij, D.G. (1993). A quantitative study of spermatogonial multiplication and stem cell renewal in the C3H/101 F1 hybrid mouse. Mutat. Res. Mol. Mech. Mutagen. *290*, 193–200.

Takahashi, J.S. (2016). Transcriptional architecture of the mammalian circadian clock. Nat. Rev. Genet. *18*, 164.

Takahashi, J.S., Shimomura, K., and Kumar, V. (2008). Searching for Genes Underlying Behavior: Lessons from Circadian Rhythms. Science *322*, 909–912.

Tatsuki, F., Sunagawa, G.A., Shi, S., Susaki, E.A., Yukinaga, H., Perrin, D., Sumiyama, K., Ukai-Tadenuma, M., Fujishima, H., Ohno, R., et al. (2016). Involvement of Ca 2+ -Dependent Hyperpolarization in Sleep Duration in Mammals. Neuron *90*, 70–85.

Tomita, J., Ban, G., and Kume, K. (2017). Genes and neural circuits for sleep of the fruit fly. Neurosci. Res. *118*, 82–91.

Uebi, T., Itoh, Y., Hatano, O., Kumagai, A., Sanosaka, M., Sasaki, T., Sasagawa, S., Doi, J., Tatsumi, K., Mitamura, K., et al. (2012). Involvement of SIK3 in glucose and lipid homeostasis in mice. PLoS One *7*.

Vitaterna, M.H., King, D.P., Chang, A.M., Kornhauser, J.M., Lowrey, P.L., McDonald, J.D., Dove, W.F., Pinto, L.H., Turek, F.W., and Takahashi, J.S. (1994). Mutagenesis and mapping of a mouse gene, Clock, essential for circadian behavior. Science *264*, 719–725.

Vitaterna, M.H., Pinto, L.H., and Takahashi, J.S. (2006). Large-scale mutagenesis and phenotypic screens for the nervous system and behavior in mice. Trends Neurosci. *29*, 233–240.

Volpe, B.T., and Ratan, R.R. (2007). Clinical and Neurobiological Aspects of Stroke Recovery. In Neurobiology of Disease, (Elsevier), pp. 241–253.

Wang, T., Zhan, X., Bu, C.-H., Lyon, S., Pratt, D., Hildebrand, S., Choi, J.H., Zhang, Z., Zeng, M., Wang, K., et al. (2015). Real-time resolution of point mutations that cause phenovariance in mice. Proc. Natl. Acad. Sci. *112*, E440–E449.

Weber, F., and Dan, Y. (2016). Circuit-based interrogation of sleep control. Nature *538*, 51–59.

Wiltshire, S., Cardon, L.R., and McCarthy, M.I. (2002). Evaluating the Results of Genomewide Linkage Scans of Complex Traits by Locus Counting. Am. J. Hum. Genet. *71*, 1175–1182.

REFERENCE